entropy

IMPACT FACTOR 2.0

Indexed in: PubMed

CITESCORE 5.2

Article

Quantum Coherence and Purity in Dissipative Hydrogen Atoms: Insights from the Lindblad Master Equation

Kamal Berrada and Smail Bougouffa

Special Issue

Entropy in Classical and Quantum Information Theory with Applications

Edited by

Dr. Dominik Szczęśniak and Prof. Dr. Sabre Kais

MDPI

https://doi.org/10.3390/e27080848

entropy

MDPI

Article

Quantum Coherence and Purity in Dissipative Hydrogen Atoms: Insights from the Lindblad Master Equation

Kamal Berrada * and Smail Bougouffa

Department of Physics, College of Science, Imam Mohammad Ibn Saud Islamic University (IMSIU), P.O. Box 90950, Riyadh 11623, Saudi Arabia; sbougouffa@imamu.edu.sa
* Correspondence: kaberrada@imamu.edu.sa

Abstract

In this work, we investigate the quantum coherence and purity in hydrogen atoms under dissipative dynamics, with a focus on the hyperfine structure states arising from the electron–proton spin interaction. Using the Lindblad master equation, we model the time evolution of the density matrix of the system, incorporating both the unitary dynamics driven by the hyperfine Hamiltonian and the dissipative effects due to environmental interactions. Quantum coherence is quantified using the L_1 norm and relative entropy measures, while purity is assessed via von Neumann entropy, for initial states, including a maximally entangled Bell state and a separable state. Our results reveal distinct dynamics: for the Bell states, both coherence and purity decay exponentially with a rate proportional to the dissipation parameter, whereas for a kind of separable state, coherence exhibits oscillatory behavior modulated via the hyperfine coupling constant, superimposed on an exponential decay, and accompanied by a steady increase in entropy. Higher dissipation rates accelerate the loss of coherence and the growth of von Neumann entropy, underscoring the environment's role in suppressing quantum superposition and driving the system towards mixed states. These findings enhance our understanding of coherence and purity preservation in atomic systems and offer insights for quantum information applications where robustness against dissipation is critical.

Keywords: hydrogen atoms; Lindblad master equation; coherence; von Neumann entropy; hyperfine Hamiltonian

check for updates

Academic Editors: Sabre Kais and Dominik Szczęśniak

Received: 21 July 2025
Revised: 4 August 2025
Accepted: 5 August 2025
Published: 10 August 2025

Citation: Berrada, K.; Bougouffa, S. Quantum Coherence and Purity in Dissipative Hydrogen Atoms: Insights from the Lindblad Master Equation. *Entropy* **2025**, *27*, 848. https://doi.org/10.3390/e27080848

Copyright: © 2025 by the authors. Licensee MDPI, Basel, Switzerland. This article is an open access article distributed under the terms and conditions of the Creative Commons Attribution (CC BY) license (https://creativecommons.org/licenses/by/4.0/).

1. Introduction

The hydrogen atom, with its elegantly simple structure, has historically served as a cornerstone of quantum mechanics understanding, offering profound insights into the behavior of electrons and nuclei in diverse physical, chemical, and biological contexts [1–4]. Beyond its foundational role in quantum theory, the hydrogen atom emerges as a pivotal element in quantum information science, providing a natural system for exploring quantum correlations. The electron and nuclear spins in the hydrogen atom offer a physically intuitive framework and a well-defined Hilbert space for investigating bipartite quantum entanglement, whose entanglement, quantified by two-qubit concurrence, can be directly linked to fundamental constants such as the Planck constant, the Boltzmann constant, electron and proton masses, the fine-structure constant, the Bohr radius, and the Bohr magneton. At low temperatures, the hyperfine structure (HFS) states of the hydrogen atom exhibit inherent entanglement, which diminishes rapidly as the temperature increases, eventually disappearing beyond a critical threshold of $\tau_c \approx 5.35\,\mu\text{eV}$. This phenomenon is

rooted in the thermal equilibrium behavior of the HFS states, where the entanglement is sensitive to the balance between the energy gap and thermal energy [5–7]. Recent studies have further revealed nuclear-polarized phases of hydrogen atoms embedded in solid H_2 films [5,8], showcasing significant deviations from the Boltzmann distribution at low temperatures [5–7], which raises intriguing questions about the role of quantum effects in such systems. The electron- and nuclear-spin degrees of freedom in the hydrogen atom provide a platform for studying entanglement and connecting to broader applications in quantum information. Earlier research on electron-spin dynamics in two-electron double-quantum-dot systems [9,10] has demonstrated the potential of such systems as qubits for quantum information technologies [11–13]. Similarly, nuclear spins, particularly in systems like nitrogen-vacancy centers in diamonds, have been identified as valuable resources for quantum information processing [14–17]. In contrast to previous works that explored electron–proton coordinate entanglement [18] or provided a formalism for HFS entanglement [19], this study uncovers a novel aspect: the ability of an external magnetic field to induce and sustain HFS entanglement even at temperatures well above the critical threshold τ_c. This magnetically induced entanglement defies the thermal degradation typically observed in such systems, offering a new avenue for entanglement engineering in low-temperature environments, including gases and solids.

Quantum coherence (QC), a phenomenon emerging from the superposition principle, constitutes a cornerstone of quantum mechanics and serves as an essential resource across a spectrum of quantum information processing applications, including quantum reference frames [20–22], quantum transport within biological systems [23–25], and quantum thermodynamics [26–28]. The task of quantifying QC represents a critical challenge both in the theoretical foundations of quantum mechanics and in the practical domain of quantum information science, drawing significant research focus in recent years [29]. This framework has notably elucidated the role of coherence in underpinning quantum advantages, such as quantum state merging [30], deterministic quantum computation with one qubit [31], the Deutsch–Jozsa algorithm [32], and Grover's search algorithm [33]. Furthermore, the resource theory of coherence provides a robust foundation for interpreting the wave-like characteristics of quantum systems [34], as well as the intrinsic nature of quantum correlations, encompassing entanglement [35] and an array of discord-like measures [36]. Baumgratz et al. [29] have recently advanced a resource-theoretic framework to systematically quantify QC in quantum states, paving the way for the development of diverse coherence measures rooted in distinct physical principles. The initial proposals included the norm of coherence and the relative entropy of coherence, both based on distance-based metrics [29]. This was followed by subsequent measures that leveraged entanglement [37], operational perspectives [38,39], and convex-roof constructions [40,41]. These quantitative tools have enabled detailed investigations into QC's multifaceted properties, such as its interconnections with other quantum resources [37,42,43], its manifestation in infinite-dimensional Hilbert spaces [44,45], its complementarity relations [46], and the quantification of macroscopic coherence [47]. This resource-theoretic approach to QC quantification has thus catalyzed a broad array of further explorations into the nature and implications of QC [48–51].

The theory of open quantum systems examines the dynamics of quantum systems that interact with their surrounding environments, a topic of significant interest since the foundational development of quantum mechanics [52]. Despite considerable theoretical progress, fundamental challenges remain unresolved, notably the phenomenon of decoherence, which involves the loss of quantum coherence due to interactions between a system and its environment.

Recent progress has considerably deepened our understanding of quantum coherence, particularly its behavior in decoherence and noisy environments. Key studies have explored phenomena such as frozen coherence, analytical evolution equations, noise coherence-generating power, and coherence dynamics in correlated channels [53–56]. These contributions provide essential tools and perspectives for analyzing coherence loss and preservation in open quantum systems.

Building on these developments, it is clear that understanding coherence dynamics is essential not only from a fundamental perspective but also for practical uses. This process has attracted substantial attention in the fields of quantum information and computation, where decoherence remains one of the central challenges in the realization of scalable quantum information processors [57–59]. The preservation of QC is indispensable for the operation of quantum computers, quantum cryptography, and quantum teleportation. Furthermore, decoherence serves as a critical mechanism for understanding the quantum-to-classical transition, wherein the emergence of classical properties from quantum systems is interpreted as a consequence of environmentally induced decoherence. In this study, we investigate the QC and purity in hydrogen atoms under dissipative dynamics using the Lindblad master equation. We will show that Bell states exhibit exponential decay in both coherence and purity, while separable states show oscillatory coherence with decay and rising entropy, effects that worsen with higher dissipation rates. The results obtained highlight the role of the environment in the degradation of the QC and purity, providing critical insights for the preservation of quantum properties in atomic systems.

This manuscript is structured as follows. Section 2 describes the system Hamiltonian and presents the solution to the physical model. In Section 3, we introduce the coherence measure and analyze its time-dependent behavior for the model under consideration. Finally, Section 4 summarizes the key findings of this study.

2. The Hamiltonian and Quantum Dynamics

The ground state of the hydrogen atom exhibits a fascinating interplay of spin degrees of freedom governed by the hyperfine interaction Hamiltonian. This Hamiltonian captures the magnetic dipole–dipole coupling between the electron and proton spins and is mathematically expressed as

$$H_{\mathrm{HF}} = A(\sigma_e \cdot \sigma_p). \tag{1}$$

Here, $\sigma_e = (\sigma_e^x, \sigma_e^y, \sigma_e^z)$ represents the vector of Pauli operators for the electron spin, while $\sigma_p = (\sigma_p^x, \sigma_p^y, \sigma_p^z)$ denotes the corresponding vector for the proton spin. These operators act on the spin-1/2 nature of both particles, encoding their quantum mechanical spin properties along the three spatial axes. The parameter A, termed the hyperfine structure constant, quantifies the strength of this interaction. It arises from a combination of fundamental physical constants, including the fine-structure constant α, which governs electromagnetic interactions; the electron and proton g-factors, g_e and g_p, which adjust the magnetic moments relative to the Bohr magneton and nuclear magneton; the vacuum permeability μ_0; the reduced Planck constant $\hbar$; the Bohr radius a_0, a measure of the electron–proton separation in the ground state; and the masses of the electron m_e and proton m_p. The precise form of this constant is given by $A = \frac{8}{3}\alpha^2 g_e g_p \frac{\mu_0}{4\pi}\frac{\hbar^2}{a_0^3}\frac{m_e}{m_p}$. This hyperfine Hamiltonian dictates the energy level structure of the hydrogen atom's ground state by coupling the electron and proton spins into a total spin system. Given that both the electron and the proton are spin-1/2 particles, their spins can either align to form a triplet configuration with total spin $S_{\mathrm{total}} = 1$ or anti-align to form a singlet configuration with $S_{\mathrm{total}} = 0$. The eigenvalues of H_{HF} reveal this splitting: the triplet states, characterized by parallel spin orientations, possess an energy of $E = A$, whereas the singlet state, with antiparallel spins, has an energy

of $E = -3A$. The energy separation between these levels, known as hyperfine splitting, is thus $\Delta E = 4A$.

The effective Hamiltonian in Equation (1) describes the hyperfine interaction in the hydrogen atom, valid when the electron occupies the ground (1*s*) state. In this regime, the dominant spin-dependent interaction is the magnetic dipole–dipole coupling between the electron and proton spins. The Coulomb binding and spin–orbit coupling are either already accounted for in the energy level structure or negligible (e.g., spin–orbit vanishes for $l = 0$).

The Hamiltonian eigenstates span a four-dimensional Hilbert space given by the computational basis $\mathcal{B} = \{|\uparrow_e\uparrow_p\rangle, |\uparrow_e\downarrow_p\rangle, |\downarrow_e\uparrow_p\rangle, |\downarrow_e\downarrow_p\rangle\}$. Here, $|\uparrow\rangle$ and $|\downarrow\rangle$ denote spin-up and spin-down states along the z-axis for the electron (subscript e) and proton (subscript p). The energy eigenvalues are derived using the total spin operator $S = S_e + S_p$. For triplet states ($S_{\text{total}} = 1$), $S^2 = 2\hbar^2$, giving energy $E = A$; for the singlet state ($S_{\text{total}} = 0$), $S^2 = 0$, giving $E = -3A$. The singlet eigenstate, $|a\rangle$, is a Bell state:

$$|a\rangle = \frac{1}{\sqrt{2}}\left(|\uparrow_e\downarrow_p\rangle - |\downarrow_e\uparrow_p\rangle\right), \tag{2}$$

with energy $E_a = -3A$. The triplet eigenstates ($E = A$) include two separable states:

$$|d\rangle = |\uparrow_e\uparrow_p\rangle, \tag{3}$$

$$|b\rangle = |\downarrow_e\downarrow_p\rangle, \tag{4}$$

with energies $E_d = E_b = A$, representing spins aligned up or down. The third triplet state, $|c\rangle$, is another entangled Bell state:

$$|c\rangle = \frac{1}{\sqrt{2}}\left(|\uparrow_e\downarrow_p\rangle + |\downarrow_e\uparrow_p\rangle\right), \tag{5}$$

with energy $E_c = A$. The presence of entangled eigenstates such as $|a\rangle$ and $|c\rangle$ within the hyperfine structure illustrates the hydrogen atom's intrinsic quantum mechanical richness. These states, alongside the separable triplet states $|b\rangle$ and $|d\rangle$, fully characterize the spin dynamics of the system in its ground state. The energy difference $\Delta E = 4A$ drives observable phenomena, such as the 21 cm spectral line. This structure not only provides insight into atomic physics but also serves as a foundational example for understanding quantum correlations in more complex systems, enabling studies of QC and von Neumann dynamics under dissipation, as explored in this work.

The system is characterized by the hyperfine Hamiltonian and dissipative interactions modeled via Lindblad operators representing spin-flip processes for the electron and proton. The time evolution of the density matrix $\rho(t)$ is governed via the Lindblad master equation, which accounts for both unitary evolution and dissipation

$$\frac{d\rho(t)}{dt} = -i[H_{\text{HF}}, \rho(t)] + \mathscr{D}(\rho(t)), \tag{6}$$

where $\mathscr{D}(\rho(t))$ is the dissipation superoperator. The dissipative term is expressed as

$$\mathscr{D}(\rho) = \frac{\gamma}{2}\sum_{k=1}^{4}\left(L_k\rho L_k^\dagger - \frac{1}{2}\{L_k^\dagger L_k, \rho\}\right), \tag{7}$$

where γ represents the dissipation rate, and L_k are the Lindblad operators describing spin-flip processes. These operators are defined as

$$L_1 = \sigma_+^e \otimes I_p, \quad \text{(electron spin-up transition)} \tag{8}$$
$$L_2 = \sigma_-^e \otimes I_p, \quad \text{(electron spin-down transition)} \tag{9}$$
$$L_3 = I_e \otimes \sigma_+^p, \quad \text{(proton spin-up transition)} \tag{10}$$
$$L_4 = I_e \otimes \sigma_-^p, \quad \text{(proton spin-down transition)} \tag{11}$$

Here, $\sigma_+ = |\uparrow\rangle\langle\downarrow|$ and $\sigma_- = |\downarrow\rangle\langle\uparrow|$ denote the raising and lowering operators for the respective spin systems. Further, we assume equal rates for the excitation and decay processes, corresponding to the high-temperature limit of a thermal reservoir, where $\bar{n} \to \infty$ and $\Gamma \to 0$, such that the product $\Gamma\bar{n} \equiv \gamma$ remains finite. This approximation leads to symmetric noise channels and is consistent with the infinite-temperature limit described in Ref. [60] (see Equation (112) and its discussion). Although we adopt equal rates for simplicity, the model can be extended to include temperature-dependent asymmetric rates, which will be explored in future work.

The time derivative $\frac{d\rho}{dt}$ yields a set of coupled differential equations for the matrix elements $\rho_{ij}(t)$, where $i, j = 1, 2, 3, 4$ correspond to the computational basis. These equations account for coherent interactions, parameterized by the coupling strength A, and dissipative processes, characterized by the dissipation rate γ. The equations are separated into those governing the diagonal elements (populations) and the off-diagonal elements (coherences) for clarity.

The diagonal elements $\rho_{ii}(t)$ represent the probabilities of finding the system in each basis state. Their time evolution is given as follows:

$$\frac{d\rho_{11}}{dt} = \gamma(\rho_{22} + \rho_{33} - 2\rho_{11}), \tag{12}$$
$$\frac{d\rho_{22}}{dt} = -2iA(\rho_{23} - \rho_{32}) + \gamma(\rho_{11} + \rho_{44} - 2\rho_{22}), \tag{13}$$
$$\frac{d\rho_{33}}{dt} = 2iA(\rho_{23} - \rho_{32}) + \gamma(\rho_{11} + \rho_{44} - 2\rho_{33}), \tag{14}$$
$$\frac{d\rho_{44}}{dt} = \gamma(\rho_{22} + \rho_{33} - 2\rho_{44}). \tag{15}$$

Here, the terms involving γ describe population transfer due to dissipation, while the terms with A in ρ_{22} and ρ_{33} arise from coherent coupling between states $|\uparrow_e\downarrow_p\rangle$ and $|\downarrow_e\uparrow_p\rangle$.

The off-diagonal elements $\rho_{ij}(t)$ (for $i \neq j$) represent the coherence between the basis states. Their dynamics are governed via the following:

$$\frac{d\rho_{12}}{dt} = -2iA(\rho_{12} - \rho_{13}) + \gamma(\rho_{34} - 2\rho_{12}), \tag{16}$$
$$\frac{d\rho_{13}}{dt} = -2iA(\rho_{13} - \rho_{12}) + \gamma(\rho_{24} - 2\rho_{13}), \tag{17}$$
$$\frac{d\rho_{14}}{dt} = -2\gamma\rho_{14}, \tag{18}$$
$$\frac{d\rho_{23}}{dt} = -2iA(\rho_{22} - \rho_{33} + \rho_{23}) - 2\gamma\rho_{23}, \tag{19}$$
$$\frac{d\rho_{24}}{dt} = -2iA(\rho_{24} - \rho_{34}) + \gamma(\rho_{13} - 2\rho_{24}), \tag{20}$$
$$\frac{d\rho_{34}}{dt} = -2iA(\rho_{24} - \rho_{34}) + \gamma(\rho_{12} - 2\rho_{34}). \tag{21}$$

These equations include both coherent evolution (terms with A) and decoherence (terms with γ). In particular, ρ_{14} decays purely dissipatively, indicating that there is no coherent

coupling between states $|\uparrow_e\uparrow_p\rangle$ and $|\downarrow_e\downarrow_p\rangle$. The remaining off-diagonal elements (ρ_{21}, ρ_{31}, ρ_{32}, ρ_{41}, ρ_{42}, ρ_{43}) are determined by Hermitian conjugation, ensuring the density matrix remains Hermitian ($\rho^\dagger = \rho$). Specifically, $\rho_{ji} = \rho_{ij}^*$ for all i, j. These differential equations fully describe the dynamics of the system under the combined effects of coherent interactions and dissipation. They can be solved analytically under specific initial conditions.

3. Quantum Coherence and Results

In the resource-theoretic framework of QC, the l_1-norm of coherence serves as a fundamental measure to quantify the coherence present in a quantum state, is given by [29]

$$C_{l_1}(\rho) = \sum_{i \neq j} |\rho_{i,j}|, \tag{22}$$

where ρ is the density matrix, and the sum captures the absolute values of its off-diagonal elements. This metric provides a straightforward and computationally efficient way to assess the magnitude of quantum superpositions, making it particularly valuable for analyzing coherence dynamics in systems like hydrogen atoms under dissipative conditions, as explored in this manuscript. Complementing this, the relative entropy of coherence, given by

$$C_{\text{rel}}(\rho) = S(\rho_{\text{diag}}) - S(\rho), \tag{23}$$

where S denotes the von Neumann entropy, and ρ_{diag} is the diagonal part of ρ, which measures coherence through the entropic difference between the incoherent (diagonal) state and the full quantum state. This information-theoretic measure effectively captures the quantum information encoded in off-diagonal terms and adheres to essential properties such as vanishing for incoherent states, monotonicity under incoherent operations, and convexity. Both measures align with the resource theory of coherence, ensuring that coherence remains a non-increasing resource under free (incoherent) operations.

Contemporary studies have shown that entropy generation within the framework of classical thermodynamics can be understood as the development of correlations between an open quantum system and its surrounding environment [61–64]. For a quantum state, ρ, representing a qubit, the von Neumann entropy is defined by the expression

$$S(\rho) = -\text{tr}(\rho \ln \rho). \tag{24}$$

In the context of a bipartite quantum system, the entropies of the individual subsystems and the combined system conform to the inequalities

$$|S(\rho_A) - S(\rho_B)| \leq S(\rho_{AB}) \leq S(\rho_A) + S(\rho_B), \tag{25}$$

where A and B designate the two distinct subsystems.

Given the initial state,

$$\cos\alpha|\uparrow_e\downarrow_p\rangle + \sin\alpha|\downarrow_e\uparrow_p\rangle, \tag{26}$$

the non-zero elements of the time-evolved density matrix $\rho(t)$ can be analytically derived from the Lindblad master equation (see Appendix A). The density matrix at time t is found to be

$$\rho(t) = \begin{pmatrix} \rho_{11}(t) & 0 & 0 & \rho_{14}(t) \\ 0 & \rho_{22}(t) & \rho_{23}(t) & 0 \\ 0 & \rho_{32}(t) & \rho_{33}(t) & 0 \\ \rho_{41}(t) & 0 & 0 & \rho_{44}(t) \end{pmatrix} \tag{27}$$

where

$$\begin{aligned}
\rho_{11}(t) &= \frac{1}{4}\left[1 - e^{-4\gamma t}\right], \\
\rho_{44}(t) &= \frac{1}{4}\left[1 - e^{-4\gamma t}\right], \\
\rho_{22}(t) &= \frac{1}{4}\left[1 + e^{-4\gamma t} + 2\cos(2\alpha)\cos(4At)e^{-2\gamma t}\right], \\
\rho_{33}(t) &= \frac{1}{4}\left[1 + e^{-4\gamma t} - 2\cos(2\alpha)\cos(4At)e^{-2\gamma t}\right], \\
\rho_{23}(t) &= \frac{1}{2}e^{-2\gamma t}[i\cos(2\alpha)\sin(4At) + \sin(2\alpha)], \\
\rho_{ij}(t) &= 0 \quad \text{for all other } i, j,
\end{aligned} \tag{28}$$

illustrating the decay of coherences and redistribution of populations over time. These solutions highlight the interplay between coherent oscillations (driven by A) and decoherence (governed by γ). The coherence between the states $|1\rangle$ and $|4\rangle$ decays exponentially with time, while the populations in the diagonal elements approach a uniform distribution due to the dissipative interactions.

In Figure 1, we present the time evolution of the L_1-norm of coherence for the electron–proton system in a hydrogen atom, initially prepared in a maximally entangled Bell state ($\alpha = \pi/4$), under dissipative dynamics modeled with the Lindblad master equation. This measure, defined as the sum of the absolute values of the off-diagonal elements of the density matrix, quantifies the QC in the system. The figure illustrates an exponential decay of the L_1-norm for dissipation parameters $\gamma = 0.1$ (solid line), $\gamma = 0.5$ (dashed line), and $\gamma = 1.0$ (dash-dotted line), with the decay rate increasing as γ grows. This behavior underscores the rapid loss of quantum superpositions due to environmental interactions, highlighting the detrimental effect of dissipation on coherence in atomic systems. Complementing this, Figure 2 depicts the time evolution of the von Neumann entropy for the same electron–proton state under identical dissipative conditions. Starting from zero for the pure Bell state, the entropy increases toward a maximum value, indicating the system's transition to a fully mixed state. The plot shows this rise for $\gamma = 0.1$ (solid line), $\gamma = 0.5$ (dashed line), and $\gamma = 1.0$ (dash-dotted line), with the rate of entropy growth accelerating with higher γ. This trend emphasizes how stronger dissipation hastens the erosion of quantum purity and correlations. Together, Figures 1 and 2 provide a comprehensive view of how dissipative dynamics undermine quantum features in hydrogen atoms. The exponential decay of the L_1-norm of coherence and the corresponding increase in von Neumann entropy reveal the challenges of maintaining quantum properties under environmental noise, critical for applications in quantum information technologies. By quantifying these effects, this study establishes a foundation for developing strategies to preserve coherence and purity in atomic systems against dissipation.

In Figure 3, we present the time evolution of the L_1-norm of coherence for the electron–proton system in a hydrogen atom, initially prepared in a separable state ($\alpha = 0$), under dissipative dynamics governed by the Lindblad master equation. The figure illustrates oscillatory behavior driven by the hyperfine coupling constant A, overlaid with an exponential decay envelope governed by the dissipation parameter $\gamma = 0.1$ (solid line), $\gamma = 0.5$ (dashed line), and $\gamma = 1.0$ (dash-dotted line). Higher values of γ accelerate the coherence loss, demonstrating the sensitivity of quantum superpositions to environmental interactions in atomic systems. Similarly, Figure 4 displays the time evolution of the L_1-norm of coherence for the electron–proton system in a hydrogen atom, initially prepared in a partially entangled state with $\alpha = \pi/3$. The system evolves under dissipative dynamics governed by the Lindblad master equation, and the plot shows the effect of different dissipation rates.

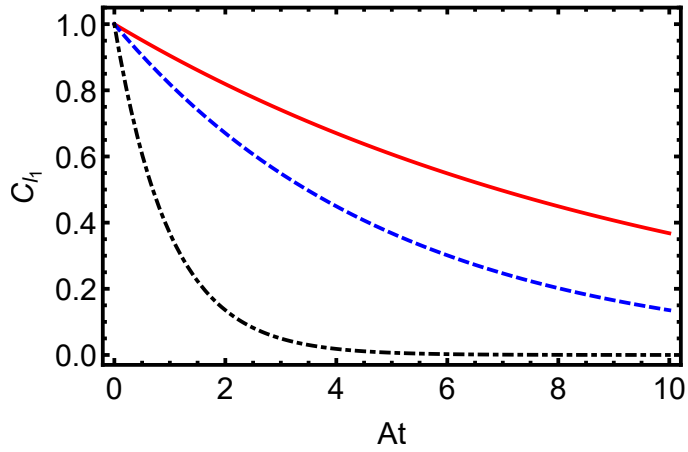

Figure 1. Time evolution of the L_1-norm of coherence for the electron–proton system in a hydrogen atom, initially prepared in a maximally entangled Bell state ($\alpha = \pi/4$), under dissipative dynamics modeled by the Lindblad master equation. The plot illustrates the coherence decay for dissipation parameters $\gamma = 0.1$ (solid line), $\gamma = 0.5$ (dashed line), and $\gamma = 1.0$ (dash-dotted line). The behavior of coherence highlights the detrimental effect of environmental interactions on QC in atomic systems, emphasizing the challenges of maintaining quantum properties under dissipation.

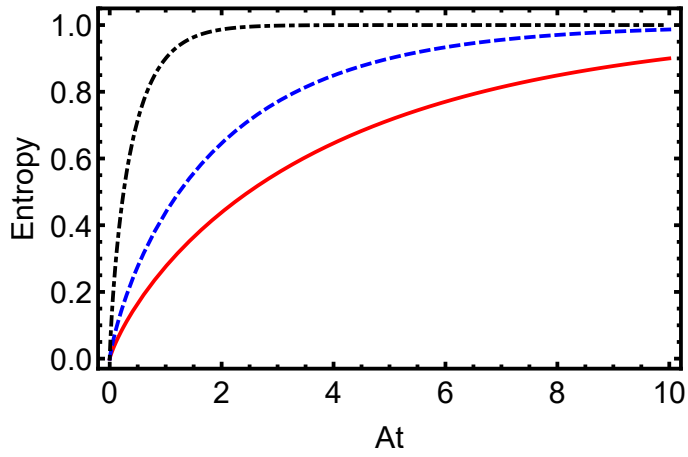

Figure 2. Time evolution of von Neumann entropy for the electron–proton state in a hydrogen atom, initially prepared in a maximally entangled Bell state ($\alpha = \pi/4$), under dissipative dynamics modeled with the Lindblad master equation. The plot illustrates the entropy increase for varying dissipation parameters $\gamma = 0.1$ (solid line), $\gamma = 0.5$ (dashed line), and $\gamma = 1.0$ (dash-dotted line). Each curve shows a rise from an initial zero entropy toward a maximum value. The rate of entropy growth accelerates with an increasing γ, underscoring the role of environmental dissipation in eroding quantum purity.

The oscillatory pattern, modulated by A, is progressively suppressed by increasing γ, underscoring the detrimental impact of dissipation on quantum resources essential for applications such as quantum computing. Complementing these observations, Figure 5 depicts the time evolution of von Neumann entropy, an indicator of the system's quantum purity. Starting from a low initial value for the separable state, the entropy rises steadily toward a maximum, signaling the system's progression toward a more mixed state in the long-time limit, though not reaching the maximally mixed state, $I_4/4$, for which $S(\rho) = \ln(4) \approx 1.3863$.The rate of this increase is directly tied to γ, with stronger dissipation hastening the loss of purity. Collectively, Figures 3–5 illustrate how dissipative dynamics degrade key quantum features, coherence and purity, in hydrogen atoms. Despite the different initial states—with Figure 2 starting from a maximally entangled Bell state and Figure 5 from a separable state—the behavior of von Neumann entropy is remarkably simi-

lar in both cases. This similarity indicates that the entropy's increase toward its maximum value, signaling the transition to a fully mixed state, is independent of the initial state of the system. Such behavior underscores the universal role of dissipation in eroding quantum purity, regardless of the system's starting configuration. On the other hand, it is worth noting that coherence and mixedness are not independent quantities: for a given quantum state, ρ, the l_1 norm of coherence $C_{l_1}(\rho)$ and the linear mixedness $M_l(\rho) = \frac{d}{d-1}(1 - \mathrm{Tr}[\rho^2])$ satisfy a tradeoff relation, as discussed in [65,66]. This means that, as the system becomes more mixed (higher M_l), coherence tends to decrease, a behavior that is consistent with our numerical observations.

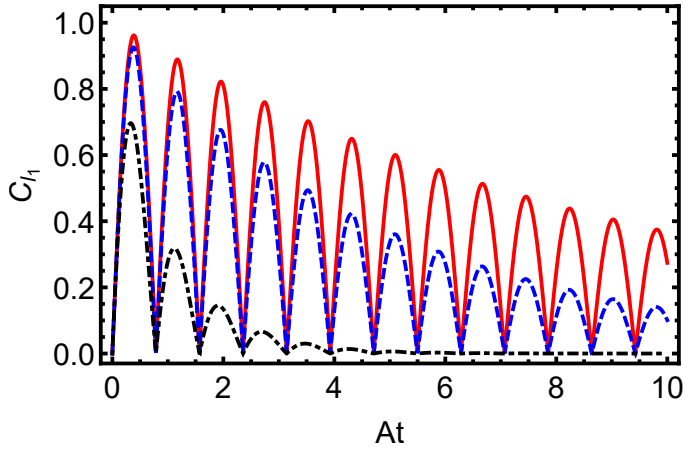

Figure 3. Time evolution of the L_1-norm of coherence for the electron–proton system in a hydrogen atom, initially prepared in a separable state ($\alpha = 0$), under dissipative dynamics governed by the Lindblad master equation. The plot illustrates the coherence dynamics for varying dissipation parameters $\gamma = 0.1$ (solid line), $\gamma = 0.5$ (dashed line), and $\gamma = 1.0$ (dash-dotted line). Each curve displays oscillatory behavior driven by the hyperfine coupling constant, A, overlaid on an exponential decay envelope influenced by γ.

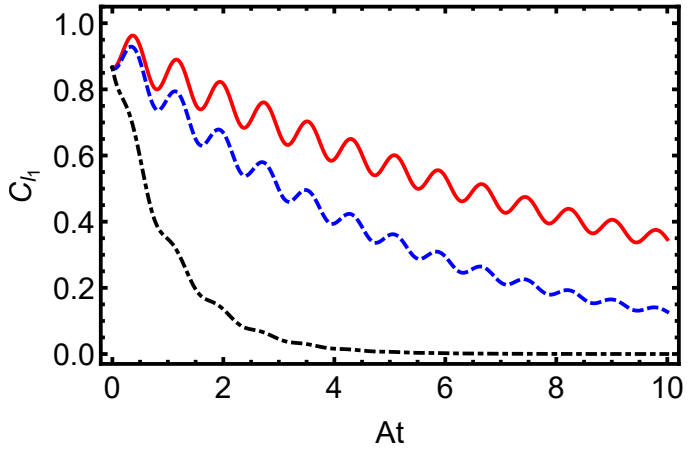

Figure 4. Time evolution of the L_1-norm of coherence for the electron–proton system in a hydrogen atom, initially in a partially entangled state ($\alpha = \pi/3$), under dissipative dynamics governed by the Lindblad master equation. The coherence dynamics are shown for dissipation parameters $\gamma = 0.1$ (solid line), $\gamma = 0.5$ (dashed line), and $\gamma = 1.0$ (dash-dotted line). The plot illustrates the coherence decay for dissipation parameters $\gamma = 0.1$ (solid red line), $\gamma = 0.5$ (dashed blue line), and $\gamma = 1.0$ (dash-dotted black line). The behavior of coherence highlights the detrimental effect of environmental interactions on QC in atomic systems, emphasizing the challenges of maintaining quantum properties under dissipation.

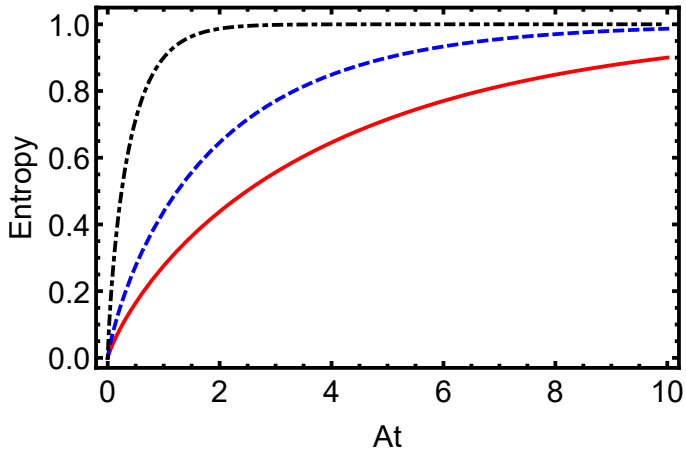

Figure 5. Time evolution of the von Neumann entropy for the electron–proton state in a hydrogen atom, initially prepared in a separable state ($\alpha = 0$), under dissipative dynamics governed by the Lindblad master equation. The plot illustrates the coherence dynamics for varying dissipation parameters $\gamma = 0.1$ (solid line), $\gamma = 0.5$ (dashed line), and $\gamma = 1.0$ (dash-dotted line). Each curve displays oscillatory behavior driven by the hyperfine coupling constant A, overlaid on an exponential decay envelope influenced by γ.

4. Conclusions

In this paper, we have investigated the QC and purity in hydrogen atoms under dissipative dynamics, with a particular focus on the hyperfine structure states arising from electron–proton spin interactions. By employing the Lindblad master equation, we modeled the time evolution of the system's density matrix, accounting for both the unitary dynamics driven by the hyperfine Hamiltonian and the dissipative effects due to environmental interactions. QC was quantified using the L_1-norm and relative entropy measures, while purity was assessed via von Neumann entropy. We examined two distinct initial states: a maximally entangled Bell state and a separable state. The results revealed distinct dynamical behaviors, depending on the initial state. For the Bell states, both coherence and purity decayed exponentially, with the decay rate directly proportional to the dissipation parameter γ. This underscored the significant impact of environmental interactions on quantum superpositions and correlations. In contrast, for certain separable states, coherence exhibited an oscillatory behavior modulated via the hyperfine coupling constant A, superimposed on exponential decay. This oscillatory pattern was accompanied by a steady increase in entropy, indicating a gradual loss of quantum purity. Furthermore, we observed that higher dissipation rates accelerated the loss of coherence and the growth of von Neumann entropy, highlighting the environment's critical role in suppressing quantum superpositions and driving the system toward mixed states. These findings provided deeper insights into the preservation of coherence and purity in atomic systems, with important implications for quantum information applications that demand resilience against environmental noise. These results may offer practical insights for quantum information protocols, including robust state initialization, strategies for mitigating decoherence, and exploiting hyperfine interactions for encoding and manipulating qubits.

Author Contributions: Writing—original draft, K.B. and S.B.; Writing—review & editing, K.B. and S.B. All authors have read and agreed to the published version of the manuscript.

Funding: This work was supported and funded by the Deanship of Scientific Research at Imam Mohammad Ibn Saud Islamic University (IMSIU) (grant number IMSIU-DDRSP2503).

Data Availability Statement: The original contributions presented in this study are included in the article. Further inquiries can be directed to the corresponding author.

Conflicts of Interest: The authors declare no conflict of interest.

Appendix A. Derivation of the Time-Evolved Density Matrix Elements

This appendix derives the analytic solution for the time-evolved density matrix $\rho(t)$ of the hydrogen atom's hyperfine structure, starting from the initial density matrix,

$$\rho(0) = \begin{pmatrix} 0 & 0 & 0 & 0 \\ 0 & \cos^2\alpha & \cos\alpha\sin\alpha & 0 \\ 0 & \cos\alpha\sin\alpha & \sin^2\alpha & 0 \\ 0 & 0 & 0 & 0 \end{pmatrix},$$

with non-zero elements $\rho_{22}(0) = \cos^2\alpha$, $\rho_{33}(0) = \sin^2\alpha$, $\rho_{23}(0) = \cos\alpha\sin\alpha$, and $\rho_{32}(0) = \cos\alpha\sin\alpha$. The Lindblad master equation yields a set of coupled differential equations for the density matrix elements,

$$\frac{d\rho_{11}}{dt} = \gamma(\rho_{22} + \rho_{33} - 2\rho_{11}), \tag{A1}$$

$$\frac{d\rho_{22}}{dt} = -2iA(\rho_{23} - \rho_{32}) + \gamma(\rho_{11} + \rho_{44} - 2\rho_{22}), \tag{A2}$$

$$\frac{d\rho_{33}}{dt} = 2iA(\rho_{23} - \rho_{32}) + \gamma(\rho_{11} + \rho_{44} - 2\rho_{33}), \tag{A3}$$

$$\frac{d\rho_{44}}{dt} = \gamma(\rho_{22} + \rho_{33} - 2\rho_{44}), \tag{A4}$$

$$\frac{d\rho_{23}}{dt} = -2iA(\rho_{22} - \rho_{33} + \rho_{23}) - 2\gamma\rho_{23}, \tag{A5}$$

with $\rho_{32}(t) = \rho_{23}^*(t)$ due to the Hermitian property of $\rho(t)$. Other off-diagonal elements, such as ρ_{14}, are found to remain zero under the given dynamics, consistent with the initial condition $\rho_{14}(0) = 0$. To solve these equations, define $s(t) = \rho_{22}(t) + \rho_{33}(t)$. When Equations (A2) and (A3) are summed, the coherent terms cancel since $\rho_{23} - \rho_{32} = 2i\mathrm{Im}(\rho_{23})$, yielding

$$\frac{ds}{dt} = 2\gamma(\rho_{11} + \rho_{44} - s).$$

Since $\mathrm{Tr}[\rho(t)] = \rho_{11} + \rho_{22} + \rho_{33} + \rho_{44} = 1$, we have $\rho_{11} + \rho_{44} = 1 - s$. Thus,

$$\frac{ds}{dt} = 2\gamma(1 - s - s) = 2\gamma(1 - 2s).$$

Solving with the initial condition $s(0) = \cos^2\alpha + \sin^2\alpha = 1$, we obtain the following:

$$s(t) = \frac{1}{2} + \frac{1}{2}e^{-4\gamma t}.$$

Since $\rho_{11} + \rho_{44} = 1 - s = \frac{1}{2}(1 - e^{-4\gamma t})$, and noting the symmetry in Equations (A1) and (A4) with $\rho_{11}(0) = \rho_{44}(0) = 0$, we find

$$\rho_{11}(t) = \rho_{44}(t) = \frac{1}{4}(1 - e^{-4\gamma t}).$$

Define $d(t) = \rho_{22}(t) - \rho_{33}(t)$ and $\rho_{23}(t) = c(t) = c_r(t) + ic_i(t)$. The system becomes the following:

$$\frac{dd}{dt} = -2\gamma d - 8Ac_i, \tag{A6}$$

$$\frac{dc_r}{dt} = 2Ac_i - 2\gamma c_r, \tag{A7}$$

$$\frac{dc_i}{dt} = -2A(d + c_r) - 2\gamma c_i, \tag{A8}$$

with initial conditions $d(0) = \cos^2\alpha - \sin^2\alpha = \cos 2\alpha$, $c_r(0) = \cos\alpha \sin\alpha = \frac{1}{2}\sin 2\alpha$, and $c_i(0) = 0$. Solving this coupled system analytically, we find that the coherent dynamics introduce oscillations at frequency $4A$, modulated by dissipative decay. The solutions are

$$\rho_{22}(t) = \frac{1}{4}\left[1 + e^{-4\gamma t} + 2\cos(2\alpha)\cos(4At)e^{-2\gamma t}\right], \tag{A9}$$

$$\rho_{33}(t) = \frac{1}{4}\left[1 + e^{-4\gamma t} - 2\cos(2\alpha)\cos(4At)e^{-2\gamma t}\right], \tag{A10}$$

$$\rho_{23}(t) = \frac{1}{2}e^{-2\gamma t}[i\cos(2\alpha)\sin(4At) + \sin(2\alpha)]. \tag{A11}$$

The conjugate $\rho_{32}(t) = \rho_{23}^*(t) = \frac{1}{2}e^{-2\gamma t}[-i\cos(2\alpha)\sin(4At) + \sin(2\alpha)]$.

References

1. Bohr, N. On the constitution of atoms and molecules. *Philos. Mag.* **1913**, *26*, 1. [CrossRef]
2. Bethe, H.; Salpeter, E. *Quantum Mechanics of One- and Two-Electron Atoms*; Springer: Berlin, Germany, 1957.
3. Series, G.W. *Spectrum of Atomic Hydrogen*; Oxford University: New York, NY, USA, 1957.
4. Landau, L.D.; Lifshitz, E.M. *Quantum Mechanics: Nonrelativistic Theory*; Pergamon: London, UK, 1958.
5. Sheludiakov, S.; McColgan, P.T.; Lee, D.M.; Khmelenko, V.V.; Järvinen, J.; Ahokas, J.; Vasiliev, S. Polarized Phases of H Atoms Embedded in Solid H_2 Films. *Phys. Rev. Lett.* **2019**, *122*, 225301. [CrossRef] [PubMed]
6. Ahokas, J.; Vainio, O.; Novotny, S.; Järvinen, J.; Khmelenko, V.V.; Lee, D.M.; Vasiliev, S. Magnetic resonance study of H atoms in thin films of H_2 at temperatures below 1 K. *Phys. Rev. B* **2010**, *81*, 104516. [CrossRef]
7. Ahokas, J.; Järvinen, J.; Khmelenko, V.V.; Lee, D.M.; Vasiliev, S. Exotic Behavior of Hydrogen Atoms in Solid H_2 at Temperatures below 1 K. *Phys. Rev. Lett.* **2006**, *97*, 095301. [CrossRef] [PubMed]
8. Bigelow, N.P.; Freed, J.H.; Lee, D.M. Nuclear-spin waves in polarized atomic hydrogen gas: Temperature and density dependence in the hydrodynamic and Knudsen regimes. *Phys. Rev. Lett.* **1989**, *63*, 1609. [CrossRef]
9. Johnson, A.C.; Petta, J.R.; Taylor, J.M.; Yacoby, A.; Lukin, M.D.; Marcus, C.M.; Hanson, M.P.; Gossard, A.C. Triplet–singlet spin relaxation via nuclei in a double quantum dot. *Nature* **2005**, *435*, 925. [CrossRef]
10. Petta, J.R.; Johnson, A.C.; Taylor, J.M.; Laird, E.A.; Yacoby, A.; Lukin, M.D.; Marcus, C.M.; Hanson, M.P.; Gossard, A.C. Coherent manipulation of coupled electron spins in semiconductor quantum dots. *Science* **2005**, *309*, 2180. [CrossRef]
11. Taylor, J.M.; Engel, H.A.; Dür, W.; Yacoby, A.; Marcus, C.M.; Zoller, P.; Lukin, M.D. Fault-tolerant architecture for quantum computation using electrically controlled semiconductor spins. *Nat. Phys.* **2005**, *1*, 177. [CrossRef]
12. Ladd, T.D.; Jelezko, F.; Laflamme, R.; Nakamura, Y.; Monroe, C.; O'Brien, J.L. Quantum computers. *Nature* **2010**, *464*, 45. [CrossRef] [PubMed]
13. Bennett, C.H.; DiVincenzo, D.P. Quantum information and computation. *Nature* **2000**, *404*, 247. [CrossRef]
14. Childress, L.; Gurudev Dutt, M.V.; Taylor, J.M.; Zibrov, A.S.; Jelezko, F.; Wrachtrup, J.; Hemmer, P.R.; Lukin, M.D. Coherent dynamics of coupled electron and nuclear spin qubits in diamond. *Science* **2006**, *314*, 281. [CrossRef] [PubMed]
15. Dutt, M.V.G.; Childress, L.; Jiang, L.; Togan, E.; Maze, J.; Jelezko, F.; Zibrov, A.S.; Hemmer, P.R.; Lukin, M.D. Quantum register based on individual electronic and nuclear spin qubits in diamond. *Science* **2007**, *316*, 1312. [CrossRef]
16. Neumann, P.; Mizuochi, N.; Rempp, F.; Hemmer, P.; Watanabe, H.; Yamasaki, S.; Jacques, V.; Gaebel, T.; Jelezko, F.; Wrachtrup, J. Multipartite entanglement among single spins in diamond. *Science* **2008**, *320*, 1326. [CrossRef]
17. Fuchs, G.D.; Dobrovitski, V.V.; Toyli, D.M.; Heremans, F.J.; Awschalom, D.D. Gigahertz dynamics of a strongly driven single quantum spin. *Science* **2009**, *326*, 1520. [CrossRef] [PubMed]

18. Tommassini, P.; Timmermans, E.; de Toledo Piza, A.F.R. The hydrogen atom as an entangled electron–proton system. *Am. J. Phys.* **1998**, *66*, 881. [CrossRef]
19. Zhu, G.; Du, K.; Li, Y. Electron-nuclear entanglement in hydrogen atom. *Phys. A* **2005**, *346*, 295. [CrossRef]
20. Bartlett, S.D.; Rudolph, T.; Spekkens, R.W. Reference frames, superselection rules, and quantum information. *Rev. Mod. Phys.* **2007**, *79*, 555. [CrossRef]
21. Marvian, I.; Spekkens, R.W. The theory of manipulations of pure state asymmetry: I. Basic tools, equivalence classes and single copy transformations. *New J. Phys.* **2013**, *15*, 033001. [CrossRef]
22. Marvian, I.; Spekkens, R.W. Modes of asymmetry: The application of harmonic analysis to symmetric quantum dynamics and quantum reference frames. *Phys. Rev. A* **2014**, *90*, 062110. [CrossRef]
23. Lloyd, S. Quantum coherence in biological systems. *J. Phys. Conf. Ser.* **2011**, *302*, 012037. [CrossRef]
24. Li, C.-M.; Lambert, N.; Chen, Y.-N.; Chen, G.-Y.; Nori, F. Witnessing quantum coherence: From solid-state to biological systems. *Sci. Rep.* **2012**, *2*, 885. [CrossRef] [PubMed]
25. Lambert, N.; Chen, Y.-N.; Chen, Y.-C.; Li, C.-M.; Chen, G.-Y.; Nori, F. Quantum biology. *Nat. Phys.* **2013**, *9*, 10. [CrossRef]
26. Narasimhachar, V.; Gour, G. Low-temperature thermodynamics with quantum coherence. *Nat. Commun.* **2015**, *6*, 7689. [CrossRef]
27. Aberg, J. Catalytic coherence. *Phys. Rev. Lett.* **2014**, *113*, 150402. [CrossRef] [PubMed]
28. Ćwikliński, P.; Studziński, M.; Horodecki, M.; Oppenheim, J. Limitations on the evolution of quantum coherences: Towards fully quantum second laws of thermodynamics. *Phys. Rev. Lett.* **2015**, *115*, 210403. [CrossRef] [PubMed]
29. Baumgratz, T.; Cramer, M.; Plenio, M.B. Quantifying coherence. *Phys. Rev. Lett.* **2014**, *113*, 140401. [CrossRef]
30. Horodecki, M.; Oppenheim, J.; Winter, A. Partial quantum information. *Nature* **2005**, *436*, 673. [CrossRef]
31. Knill, E.; Laflamme, R. Power of one bit of quantum information. *Phys. Rev. Lett.* **1998**, *81*, 5672. [CrossRef]
32. Deutsch, D.; Jozsa, R. Rapid solution of problems by quantum computation. *Proc. R. Soc. Lond. A* **1992**, *439*, 553.
33. Grover, L.K. Super classical search algorithm to find an element in unsorted array. *Phys. Rev. Lett.* **1996**, *79*, 325. [CrossRef]
34. Marletto, C.; Vedral, V. Gravitationally Induced Entanglement between Two Massive Particles is Sufficient Evidence of Quantum Effects in Gravity. *Phys. Rev. Lett.* **2017**, *119*, 040402. [CrossRef]
35. Hu, M.-L.; Hu, X.; Wang, J.; Peng, Y.; Zhang, Y.-R.; Fan, H. Quantum coherence and geometric quantum discord. *Phys. Rep.* **2018**, *762–764*, 1–100. [CrossRef]
36. Adesso, G.; Bromley, T.R.; Cianciaruso, M. Measures and applications of quantum correlations. *J. Phys. A Math. Theor.* **2016**, *49*, 473001. [CrossRef]
37. Streltsov, A.; Singh, U.; Dhar, H.S.; Bera, M.N.; Adesso, G. Measuring quantum coherence with entanglement. *Phys. Rev. Lett.* **2015**, *115*, 020403. [CrossRef] [PubMed]
38. Winter, A.; Yang, D. Operational resource theory of coherence. *Phys. Rev. Lett.* **2016**, *116*, 120404. [CrossRef]
39. Chitambar, E.; Streltsov, A.; Rana, S.; Bera, M.N.; Adesso, G.; Lewenstein, M. Assisted distillation of quantum coherence. *Phys. Rev. Lett.* **2016**, *116*, 070402. [CrossRef]
40. Yuan, X.; Zhou, H.; Cao, Z.; Ma, X. Intrinsic randomness as a measure of quantum coherence. *Phys. Rev. A* **2015**, *92*, 022124. [CrossRef]
41. Du, S.; Bai, Z.; Qi, X. Coherence measures and optimal conversion for coherent states. *Quantum Inf. Comput.* **2015**, *15*, 1307. [CrossRef]
42. Yao, Y.; Xiao, X.; Ge, L.; Sun, C.P. Quantum coherence in multipartite systems. *Phys. Rev. A* **2015**, *92*, 022112. [CrossRef]
43. Xi, Z.; Li, Y.; Fan, H. Quantum coherence and correlations in quantum system. *Sci. Rep.* **2015**, *5*, 10922. [CrossRef] [PubMed]
44. Zhang, Y.-R.; Shao, L.-H.; Li, Y.; Fan, H. Quantifying coherence in infinite-dimensional systems. *Phys. Rev. A* **2016**, *93*, 012334. [CrossRef]
45. Xu, J. Quantifying coherence of Gaussian states. *Phys. Rev. A* **2016**, *93*, 032111. [CrossRef]
46. Cheng, S.; Hall, M.J.W. Complementarity relations for quantum coherence. *Phys. Rev. A* **2015**, *92*, 042101. [CrossRef]
47. Yadin, B.; Vedral, V. General framework for quantum macroscopicity in terms of coherence. *Phys. Rev. A* **2016**, *93*, 022122. [CrossRef]
48. Marvian, I.; Spekkens, R.W. Extending Noether's theorem by quantifying the asymmetry of quantum states. *Nat. Commun.* **2014**, *5*, 3821. [CrossRef]
49. Monras, A.; Chęcinska, A.; Ekert, A. Witnessing quantum coherence in the presence of noise. *New J. Phys.* **2014**, *16*, 063041. [CrossRef]
50. Karpat, G.; Çakmak, B.; Fanchini, F.F. Quantum coherence and uncertainty in the anisotropic XY chain. *Phys. Rev. B* **2014**, *90*, 104431. [CrossRef]
51. Berrada, K.; Bougouffa, S. Robustness of quantum correlations in photonic systems under non-Markovian dephasing: Theoretical analysis in the experimental range. *Sci. Rep.* **2025**, *15*, 22260. [CrossRef] [PubMed]
52. von Neumann, J. *Mathematical Foundations of Quantum Mechanics*; Princeton University Press: Princeton, NJ, USA, 1955.
53. Bromley, T.R.; Cianciaruso, M.; Adesso, G. Frozen quantum coherence. *Phys. Rev. Lett.* **2015**, *114*, 210401. [CrossRef]

54. Hu, M.-L.; Fan, H. Evolution equation for quantum coherence. *Sci. Rep.* **2016**, *6*, 29260. [CrossRef]
55. Styliaris, G.; Venuti, L.C.; Zanardi, P. Coherence-generating power of quantum dephasing processes. *Phys. Rev. A* **2018**, *97*, 032304. [CrossRef]
56. Hu, M.-L.; Fan, H. Quantum coherence of multiqubit states in correlated noisy channels. *Sci. China Phys. Mech. Astron.* **2020**, *63*, 230322. [CrossRef]
57. Nielsen, M.A.; Chuang, I.L. *Quantum Computation and Quantum Information*; Cambridge University Press: Cambridge, UK, 2000.
58. Benatti, F.; Floreanini, R. *Open Quantum Systems*; Springer: Berlin, Germany, 2003.
59. Preskill, J. *Quantum Information and Computation*; Lecture Notes for Physics 229; California Institute of Technology: Pasadena, CA, USA, 1998.
60. Mintert, F.; Kuś, M.; Buchleitner, A. Concurrence of mixed multipartite quantum states. *Phys. Rep.* **2005**, *415*, 207–275. [CrossRef]
61. Hilt, S.; Lutz, E. System-bath entanglement in quantum thermodynamics. *Phys. Rev. A* **2009**, *79*, 010101. [CrossRef]
62. Pernice, A.; Strunz, W.T. Decoherence and the nature of system-environment correlations. *Phys. Rev. A* **2011**, *84*, 062121. [CrossRef]
63. Iyoda, E.; Kaneko, K.; Sagawa, T. Fluctuation theorem for many-body pure quantum states. *Phys. Rev. Lett.* **2017**, *119*, 100601. [CrossRef] [PubMed]
64. Li, S.-W. Production rate of the system-bath mutual information. *Phys. Rev. E* **2017**, *96*, 012139. [CrossRef] [PubMed]
65. Singh, U.; Bera, M.N.; Dhar, H.S.; Pati, A.K. Maximally coherent mixed states: Complementarity between maximal coherence and mixedness. *Phys. Rev. A* **2015**, *91*, 052115. [CrossRef]
66. Faghihi, M.J.; Tavassoly, M.K. Quantum mutual entropy, coherence and correlation in the presence of phase damping. *J. Phys. B At. Mol. Opt. Phys.* **2015**, *48*, 165502.

Disclaimer/Publisher's Note: The statements, opinions and data contained in all publications are solely those of the individual author(s) and contributor(s) and not of MDPI and/or the editor(s). MDPI and/or the editor(s) disclaim responsibility for any injury to people or property resulting from any ideas, methods, instructions or products referred to in the content.